Exact Monte Carlo time dynamics in many-body lattice quantum systems

Massimo Ostilli[1,2] **and Carlo Presilla**[1,2,3]

[1] Dipartimento di Fisica, Università di Roma 'La Sapienza', Piazzale A Moro 2, Roma 00185, Italy
[2] Center for Statistical Mechanics and Complexity, Istituto Nazionale per la Fisica della Materia, Unità di Roma 1, Roma 00185, Italy
[3] Istituto Nazionale di Fisica Nucleare, Sezione di Roma 1, Roma 00185, Italy

Abstract
On the basis of a Feynman–Kac-type formula involving Poisson stochastic processes, a Monte Carlo algorithm has recently been introduced, which describes exactly the real- or imaginary-time evolution of many-body lattice quantum systems. We extend this algorithm to the exact simulation of time-dependent correlation functions. The techniques generally employed in Monte Carlo simulations to control fluctuations, namely reconfigurations and importance sampling, are adapted to the present algorithm and their validity is rigorously proved. We complete the analysis by several examples for the hard-core boson Hubbard model and for the Heisenberg model.

PACS numbers: 02.50.−r, 02.70.Ss

(Some figures in this article are in colour only in the electronic version)

1. Introduction

Probabilistic techniques, such as the quantum Monte Carlo (QMC) algorithms, provide an essential tool to investigate the properties of many-body systems. Basically, with these techniques one evaluates functions of matrices by a random walk in the space of the matrix indices [1]. Given the Hamiltonian H of the system, the idea is to find an appropriate stochastic representation of the imaginary time evolution operator $U(t) = \exp(-Ht)$ applied to some initial trial state. By using these methods, one can obtain, at least in the absence of a sign problem, the ground-state properties with a numerical effort that grows with some power of the size L of the system. On the other hand, the exact diagonalization of the Hamiltonian would imply an effort exponentially growing with L.

From a more physical point of view, a probabilistic representation provides a dual picture of the quantum systems: on one hand, the traditional description in terms of bra, ket and

operators, on the other hand, a description in terms of expectations of suitable stochastic functionals, which are averages over virtual trajectories of the particles. It is this mapping with a (in a sense) classical system that allows us to extract quantum information by statistical simulations.

In recent years, it has been proved that the dynamics of a system of quantum particles on a lattice admits an exact probabilistic representation [2–4]. A suitable stochastic functional $\mathcal{M}_{n_0}^{[0,t)}$, which is defined in terms of a collection of independent Poisson processes and diffuses from a Fock state n_0 to a Fock state n_t, has the property that the expectation value $\mathsf{E}\big(\mathcal{M}_{n_0}^{[0,t)}\delta_{n_t,n}\big)$, taken with respect to the Poisson processes, gives the matrix element of $U(t)$ between the two Fock states n_0 and n. In the theory of stochastic processes, this probabilistic representation may be regarded as the lattice version of the Feynman–Kac formula. We emphasize that in this method no approximation is introduced and no 'infinity path integral extrapolation' is requested. It will be referred to as the exact probabilistic representation (EPR) of the evolution operator $U(t)$. The validity of EPR is not limited to Hamiltonian systems: it can be used to express any imaginary- or real-time evolution operator $U(t)$ having any finite matrix H as generator.

In [5] we used EPR to obtain semi-analytical results in the limit $t \to \infty$, in which a central limit theorem applies. In this paper, we consider EPR at arbitrary times within a Monte Carlo approach (EPRMC).

Two other well-known QMC algorithms, namely the path integral Monte Carlo method (PIMC) and the Green function Monte Carlo method (GFMC), have affinities with EPRMC and a comparison is mandatory.

In PIMC, one evaluates the matrix elements of $U(t)$ by using the Trotter approximation [6]. The operator $U(t)$ is factorized in the kinetic, $\exp(-Tt)$, and interaction, $\exp(-Vt)$, terms so that one gets $\exp(-Ht) = \prod_{k=1}^{N} \exp(-Tt/N)\exp(-Vt/N) + \mathcal{O}([T,V]t^2/N^2)$. This approximation leads to a Feynman–Kac formula, in which, as in EPRMC, the trajectories in the Fock space are generated only by the kinetic part, $\exp(-Tt/N)$. However, in contrast to EPRMC, there are no stochastic times related to Poisson processes. The PIMC simulations are performed by evolving the trajectories for N steps. The drawback is that to obtain results corresponding to $t/N \to 0$, in which the Trotter approximation becomes exact, one must use extrapolation procedures. For any finite value of N, the extrapolation becomes unreliable for values of t sufficiently large. This is particularly evident in the case of real times ($t \to \mathrm{i}t$), when the matrix elements of U have an oscillating behaviour with respect to t. In contrast, no small time-step approximation is introduced in EPRMC and no extrapolation is requested.

Now, let us consider GFMC. The method consists of repeated statistical applications of the operator $(1 - Ht/N)$ to an initial state. For $N \to \infty$, one reproduces the operator $U(t)$, whereas an approximation affected by a relative error $\varepsilon(N)$ is obtained for any finite N. It is plausible that sampling directly the operator $U(t)$ instead of $(1 - Ht/N)^N$ leads to a higher efficiency. In the appendix, we show that the relative efficiency between EPRMC and GFMC in filtering the ground state is $E_0^2 \big/ \big[2E_0^{(0)}(E_1 - E_0)\varepsilon \big]$, where E_0 and E_1 are the energies of the ground- and first-excited states of the considered system and $E_0^{(0)}$ is the ground-state energy of the associated non-interacting system. Since the gap $(E_1 - E_0)$ decreases as the size L of the system is increased, compared to GFMC, EPRMC offers a more powerful method to investigate the ground-state properties of large lattice systems.

Actually, the GFMC scheme mentioned above is rather crude. Trivedi and Ceperley [7] introduced Poisson processes as a tool to obtain a more efficient GFMC method when the transition probabilities, proportional to the matrix elements of Ht/N, vanish for $N \to \infty$. We will refer to this improved GFMC as GFMCP. In [4] it has been proved that in the limit $N \to \infty$ GFMCP becomes equivalent to EPRMC. However, as explained in the appendix, for

a finite value of N the relative efficiency of EPRMC with respect to GFMCP is $\left(E_0/E_0^{(0)}\right)^2/2\varepsilon$, i.e. it is proportional to the accuracy ε^{-1} required in the approximated GFMCP.

Controlling the large fluctuations is one of the most important issues of any Monte Carlo method. This is evident in GFMC where an iterated statistical application of the operator $(1 - Ht/N)$ is performed. Roughly speaking, after k iterations one has fluctuations that grow like Δ^k, Δ being the statistical error associated with a single step. To solve the problem of large fluctuations, besides the development of the importance sampling method [6], remarkable progress has been made with the reconfiguration technique introduced by Hetherington [8] and subsequently improved by Sorella [9] who proposed a scheme without bias (see also [10]).

In this paper, after introducing some relevant physical models (section 2) and recalling EPR (section 3), we extend EPR to the study of exact time-dependent correlation functions (section 4). In the core section 5, we discuss the EPRMC algorithm first with a pure sampling and then adding fluctuation control by reconfigurations and importance sampling. A detailed proof of the validity of the reconfiguration method is given in section 6. Results of numerical simulations for the hard-core boson Hubbard model and for the Heisenberg model are discussed in section 7. Conclusions are drawn in section 8.

2. Models

The Hamiltonian models of interest have the following general structure (we shall always take $\hbar = 1$),

$$H = T + V, \tag{1}$$

where V is the potential energy operator and T the kinetic energy operator, which on a lattice assumes the form

$$T = - \sum_{i<j\in\Lambda} \sum_{\sigma=\uparrow\downarrow} \eta_{ij}\left(c_{i\sigma}^{\dagger}c_{j\sigma} + c_{j\sigma}^{\dagger}c_{i\sigma}\right). \tag{2}$$

Here $\Lambda \subset Z^d$ is a finite d-dimensional lattice with $|\Lambda|$ ordered sites and $c_{i\sigma}$ the commuting or anticommuting destruction operators at site i and spin index σ with the property $c_{i\sigma}^2 = 0$ (fermion or hard-core boson systems). The system is described in terms of Fock states labelled by the configuration $n = (n_{1\uparrow}, n_{1\downarrow}, \ldots, n_{|\Lambda|\uparrow}, n_{|\Lambda|\downarrow})$, i.e. the set of lattice occupation numbers taking the value 0 or 1. The total number of particles is $N_\sigma = \sum_{i\in\Lambda} n_{i\sigma}$ for $\sigma = \uparrow\downarrow$. We shall use the mod 2 addition $n \oplus n' = (n + n') \bmod 2$.

The analysis we develop in the following is valid for an arbitrary functional form of the potential V. However, numerical examples will be limited to the well-known Hubbard potential [11]

$$V = \sum_{i\in\Lambda} \gamma_i c_{i\uparrow}^{\dagger}c_{i\uparrow}c_{i\downarrow}^{\dagger}c_{i\downarrow}. \tag{3}$$

We emphasize that, independently of its form, V is diagonal in the Fock space, whereas T is off diagonal.

In this paper we will consider only hard-core boson systems. We recall that, even if fermion systems, such as the Hubbard model, are more attractive, hard-core bosons have not a purely academic interest. Besides the description of boson particles with a hard-core interaction, they can be mapped onto systems of half-integer spin [1, 7, 12]. As an example, we consider the $S = \frac{1}{2}$ Heisenberg quantum antiferromagnetic model

$$H = J\sum_{\langle i,j\rangle} \mathbf{S}_i \cdot \mathbf{S}_j = \frac{J}{2}\sum_{\langle i,j\rangle}\left(S_i^+ S_j^- + S_i^- S_j^+\right) + J\sum_{\langle i,j\rangle} S_i^z S_j^z, \tag{4}$$

where $J > 0$, $\langle i, j \rangle$ indicates that the sites i and j are nearest neighbours, and S_i and S_j are the spin operators. It is convenient to view the left and right factors in $S_i \cdot S_j$ as the spin operators of two sublattices A and B, respectively. The mapping is then established as follows. The operators S_i^+ and S_j^- commute on different sites and are thus identified with boson operators via $b_i^\dagger = S_i^+$ and $b_j = S_j^-$. Furthermore as $S_i^z = S_i^+ S_i^- - \frac{1}{2}$, one has $S_i^z = n_i - \frac{1}{2}$, where $n_i = b_i^\dagger b_i$ is the number operator. For a half-spin system $S_i^+ S_i^+ = S_i^- S_i^- = 0$, which implies $\left(b_i^\dagger\right)^2 = 0$. Therefore, the bosons have a hard core and a site can be occupied by at most one particle. In order to have a negative sign in the kinetic energy term, a further transformation is necessary. The spins on the sublattice B are rotated as $S_j^x \to -S_j^x$, $S_j^y \to -S_j^y$ and $S_j^z \to S_j^z$. Since this transformation is unitary, the commutation relations are left unchanged. The hard-core boson Hamiltonian then reads

$$H = -\frac{J}{2} \sum_{\langle i,j \rangle} \left(b_i^\dagger b_j + b_j^\dagger b_i\right) + J \sum_{\langle i,j \rangle} n_i n_j + E_N, \tag{5}$$

where $E_N = -JZ|\Lambda|/8$, Z being the number of nearest neighbours for the given lattice, e.g. $Z = 4$ for a square lattice in two dimensions.

3. Probabilistic representation

We are interested in evaluating matrix elements of the form $\langle n | e^{-Ht} | n_0 \rangle$ or $\langle n | e^{-iHt} | n_0 \rangle$ between two Fock states n_0 and n with $t \in \mathbb{R}$. As usual, we will speak of imaginary times in the former case and of real times in the latter one.

Let Γ be the set of links, i.e. the pairs (i, j) with $1 \leqslant i < j \leqslant |\Lambda|$ such that $\eta_{ij} \neq 0$. For simplicity, we will assume $\eta_{ij} = \eta$ if i and j are first neighbours and $\eta_{ij} = 0$ otherwise. For a d-dimensional lattice the number of links per spin component is $|\Gamma| = d|\Lambda|$. Let us introduce

$$\lambda_{ij\sigma}(n) \equiv \langle n \oplus \mathbf{1}_{i\sigma} \oplus \mathbf{1}_{j\sigma} | c_{i\sigma}^\dagger c_{j\sigma} + c_{j\sigma}^\dagger c_{i\sigma} | n \rangle, \tag{6}$$

$$V(n) \equiv \langle n | H | n \rangle, \tag{7}$$

where $\mathbf{1}_{i\sigma} = (0, \ldots, 0, 1_{i\sigma}, 0, \ldots, 0)$. Note that the values assumed by $\lambda_{ij\sigma}$ are 0 or 1 ($\lambda_{ij\sigma} = 0, \pm 1$ is possible in the case of fermion systems not considered here). We will call the link $(ij\sigma)$ active if $\lambda_{ij\sigma} \neq 0$. Let $\{N_{ij\sigma}^t\}$, $(i, j) \in \Gamma$, be a family of $2|\Gamma|$ independent left continuous Poisson processes with jump rate $\rho = \eta$ if $\lambda_{ij\sigma} \neq 0$ and 0 otherwise[4]. Let us now define the stochastic dynamics on the lattice. At each jump of the process $N_{ij\sigma}^t$ a particle with spin σ moves from site i to site j or vice versa. Let us indicate with $A(n)$ the number of active links in the configuration n

$$A(n) \equiv \sum_{(i,j) \in \Gamma} \sum_{\sigma = \uparrow\downarrow} |\lambda_{ij\sigma}(n)|. \tag{8}$$

The total number of jumps at time t is $N_t = \sum_{(i,j) \in \Gamma} \sum_{\sigma = \uparrow\downarrow} N_{ij\sigma}^t$. By ordering the jumps according to the times s_k, $k = 1, \ldots, N_t$, at which they take place in the interval $[0, t)$, we define a trajectory as the Markov chain $n_1, n_2, \ldots, n_{N_t}$ generated from the initial configuration n_0 by the stochastic dynamics described above. Let us call $\lambda_1, \lambda_2, \ldots, \lambda_{N_t}$, $V_1, V_2, \ldots, V_{N_t}$ and $A_1, A_2, \ldots, A_{N_t}$ the values of the matrix elements (6), (7) and (8) occurring along the trajectory, respectively. For simplicity, we will indicate the last configuration reached after N_t jumps as $n_t = n_{N_t}$. We will also use the symbols $A_0 = A(n_0)$, $V_0 = V(n_0)$ and $s_0 = 0$.

---

[4] Note that in [4] a more fundamental family of Poisson processes and stochastic functional are first introduced. Equation (10) is then derived as an effective algorithm.

According to [4], the following representation holds,

$$\langle \boldsymbol{n} | e^{-Ht} | \boldsymbol{n}_0 \rangle = \mathsf{E}\big(\delta_{n,n_t} \mathcal{M}_{\boldsymbol{n}_0}^{[0,t)}\big), \tag{9}$$

where the expectation $\mathsf{E}(\cdot)$ has to be taken with respect to the Poisson processes $N_{ij\sigma}^t$ and the stochastic functional $\mathcal{M}_{\boldsymbol{n}_0}^{[0,t)}$ is defined by

$$\mathcal{M}_{\boldsymbol{n}_0}^{[0,t)} = e^{\int_0^t [A(\boldsymbol{n}_s)\eta - V(\boldsymbol{n}_s)]\,ds}. \tag{10}$$

The subscript $\boldsymbol{n}_0$ in $\mathcal{M}_{\boldsymbol{n}_0}^{[0,t)}$ specifies the initial state. For real times an analogous representation holds

$$\langle \boldsymbol{n} | e^{-iHt} | \boldsymbol{n}_0 \rangle = \mathsf{E}\big(\delta_{n,n_t} \mathcal{M}_{\boldsymbol{n}_0}^{[0,it)}\big), \tag{11}$$

where

$$\mathcal{M}_{\boldsymbol{n}_0}^{[0,it)} = i^{N_t} e^{\int_0^t [A(\boldsymbol{n}_s)\eta - iV(\boldsymbol{n}_s)]\,ds}. \tag{12}$$

In the following, we will consider the case of imaginary times. Except when explicitly said, all the formulae are trivially extended to the case of real times.

Any ground-state quantity can be obtained from the matrix elements (9) by a proper manipulation and taking the limit $t \to \infty$. For instance, the ground-state energy is given by

$$E_0 = \lim_{t \to \infty} \frac{-\sum_n \partial_t \langle \boldsymbol{n} | e^{-Ht} | \boldsymbol{n}_0 \rangle}{\sum_n \langle \boldsymbol{n} | e^{-Ht} | \boldsymbol{n}_0 \rangle} = \lim_{t \to \infty} \frac{-\partial_t \mathsf{E}\big(\mathcal{M}_{\boldsymbol{n}_0}^{[0,t)}\big)}{\mathsf{E}\big(\mathcal{M}_{\boldsymbol{n}_0}^{[0,t)}\big)}. \tag{13}$$

It is easy to see [4] that $-\partial_t \mathsf{E}\big(\mathcal{M}_{\boldsymbol{n}_0}^{[0,t)}\big) = \mathsf{E}\big(\mathcal{M}_{\boldsymbol{n}_0}^{[0,t)} \mathcal{H}(\boldsymbol{n}_t)\big)$, where $\mathcal{H}(\boldsymbol{n}_t)$ is given by

$$\mathcal{H}(\boldsymbol{n}_t) \equiv \sum_{n'} \langle \boldsymbol{n}' | H | \boldsymbol{n}_t \rangle = -[A(\boldsymbol{n}_t)\eta - V(\boldsymbol{n}_t)]. \tag{14}$$

Equation (14) is the local energy of the last visited configuration $\boldsymbol{n}_t$. Therefore, equation (13) becomes

$$E_0 = \lim_{t \to \infty} \frac{\mathsf{E}\big(\mathcal{H}(\boldsymbol{n}_t) \mathcal{M}_{\boldsymbol{n}_0}^{[0,t)}\big)}{\mathsf{E}\big(\mathcal{M}_{\boldsymbol{n}_0}^{[0,t)}\big)}. \tag{15}$$

These identities are valid if the initial configuration $\boldsymbol{n}_0$ is such that $\langle E_0 | \boldsymbol{n}_0 \rangle \neq 0$. For a finite t, this scheme allows a good estimate of E_0 if $t \gg (E_1 - E_0)^{-1}$, where E_1 is the first-excited state of H. This implies that t must be increased by increasing the lattice size $|\Lambda|$.

4. Correlation functions

Let us consider a generic operator O. By using twice the Fock representation of the identity operator and twice equation (9) with functionals $\mathcal{M}_{\boldsymbol{n}_0}^{[0,t)}$ and $\mathcal{M}_{\boldsymbol{n}_0'}^{\prime[0,t')}$, respectively defined by two sets of independent Poisson processes $\{N_{ij\sigma}^t\}$ and $\{N_{ij\sigma}^{\prime\prime t'}\}$, we have

$$\begin{aligned}
\langle \boldsymbol{n} | e^{-Ht'} O\, e^{-Ht} | \boldsymbol{n}_0 \rangle &= \sum_{n_0'} \sum_{n''} \langle \boldsymbol{n} | e^{-Ht'} | \boldsymbol{n}_0' \rangle \langle \boldsymbol{n}_0' | O | \boldsymbol{n}'' \rangle \langle \boldsymbol{n}'' | e^{-Ht} | \boldsymbol{n}_0 \rangle \\
&= \sum_{n_0'} \sum_{n''} \mathsf{E}\big(\mathcal{M}_{\boldsymbol{n}_0'}^{\prime[0,t')} \delta_{n_{t'}',n} \langle \boldsymbol{n}_0' | O | \boldsymbol{n}'' \rangle \mathcal{M}_{\boldsymbol{n}_0}^{[0,t)} \delta_{n_t,n''}\big) \\
&= \sum_{n_0'} \mathsf{E}\big(\delta_{n_{t'}',n} \mathcal{M}_{\boldsymbol{n}_0'}^{\prime[0,t')} \langle \boldsymbol{n}_0' | O | \boldsymbol{n}_t \rangle \mathcal{M}_{\boldsymbol{n}_0}^{[0,t)}\big),
\end{aligned} \tag{16}$$

where $\boldsymbol{n}'_{t'}$ is the configuration reached at time t' starting from $\boldsymbol{n}'_0$. From this expression, we get

$$\sum_n \langle n| e^{-Ht'} O \, e^{-Ht} |n_0\rangle = \sum_n \mathsf{E}\big(\mathcal{M}'^{[0,t')}_n \langle n|O|n_t\rangle \mathcal{M}^{[0,t)}_{n_0}\big). \tag{17}$$

The ground-state quantum expectation of the operator O, assuming $\langle E_0|E_0\rangle = 1$, is, therefore,

$$\langle E_0|O|E_0\rangle = \lim_{t,t'\to\infty} \frac{\sum_n \mathsf{E}\big(\mathcal{M}'^{[0,t')}_n \langle n|O|n_t\rangle \mathcal{M}^{[0,t)}_{n_0}\big)}{\mathsf{E}\big(\mathcal{M}^{[0,t+t')}_{n_0}\big)}. \tag{18}$$

We can consider two basic cases for the operator O.

4.1. Diagonal operators

In this case, $\langle n'|O|n\rangle = \delta_{n',n} O(n)$ and equation (18) becomes

$$\langle E_0|O|E_0\rangle = \lim_{t,t'\to\infty} \frac{\mathsf{E}\big(\mathcal{M}'^{[0,t')}_{n_t} O(n_t) \mathcal{M}^{[0,t)}_{n_0}\big)}{\mathsf{E}\big(\mathcal{M}^{[0,t+t')}_{n_0}\big)}. \tag{19}$$

Note that $\mathsf{E}\big(\mathcal{M}'^{[0,t')}_{n_t} \mathcal{M}^{[0,t)}_{n_0}\big) = \mathsf{E}\big(\mathcal{M}^{[0,t+t')}_{n_0}\big)$, so that $\langle E_0|O|E_0\rangle = 1$ if O is the identity operator, whereas for a single realization of the stochastic functionals we have $\mathcal{M}'^{[0,t')}_{n_t} \mathcal{M}^{[0,t)}_{n_0} \neq \mathcal{M}^{[0,t+t')}_{n_0}$.

4.2. Off-diagonal operators

In this case, O is typically given in terms of elementary operators $O_{ij\sigma}$ connecting two different Fock states like $\langle n'|O_{ij\sigma}|n\rangle = O_{ij\sigma}(n)\delta_{n',n^{i\sigma\leftrightarrow j\sigma}}$, where $n^{i\sigma\leftrightarrow j\sigma}$ is the configuration obtained from n exchanging $n_{i\sigma}$ with $n_{j\sigma}$. Therefore, one has

$$\langle E_0|O_{ij\sigma}|E_0\rangle = \lim_{t,t'\to\infty} \frac{\mathsf{E}\big(\mathcal{M}'^{[0,t')}_{n_t^{i\sigma\leftrightarrow j\sigma}} O_{ij\sigma}(n_t) \mathcal{M}^{[0,t)}_{n_0}\big)}{\mathsf{E}\big(\mathcal{M}^{[0,t+t')}_{n_0}\big)}. \tag{20}$$

Similar expressions hold for other off-diagonal operators connecting two generic Fock states.

5. EPRMC algorithm

5.1. Pure sampling

Equations (9) and (10) lend themselves to a statistical evaluation of the matrix elements $\sum_{n'} \langle n'| e^{-Ht} |n\rangle$ via a random sampling of jump times and trajectories. As explained in [4], the practical algorithm works as follows. We start by determining the active links in the initial configuration n_0 assigned at time 0 and make an extraction with uniform distribution to decide which of them jumps first, say the link $(i_1 j_1 \sigma_1)$. We then extract the jump time s_1 according to the conditional probability density

$$p_{A_0}(s) = A_0\eta \exp(-A_0\eta s), \tag{21}$$

where A_0 is the number of active links before the first jump takes place. The contribution to $\mathcal{M}^{[0,t)}_{n_0}$ at the time of the first jump is, therefore,

$$e^{(A_0\eta - V_0)s_1}\theta(t - s_1) + e^{(A_0\eta - V_0)t}\theta(s_1 - t). \tag{22}$$

According to equation (10), the contribution of a given trajectory is then obtained by multiplying the factors corresponding to the different jumps determined in an analogous

way until the last jump takes place later than t, i.e.,

$$\mathcal{M}_{n_0}^{[0,t)} = \left(\prod_{k=1}^{N_t} e^{(A_{k-1}\eta - V_{k-1})(s_k - s_{k-1})} \right) e^{(A_{N_t}\eta - V_{N_t})(t - s_{N_t})} \tag{23}$$

if $N_t > 0$, and $\mathcal{M}_{n_0}^{[0,t)} = e^{(A_0\eta - V_0)t}$ if $N_t = 0$.

Let us consider N independent trajectories obtained as described above and let $\mathcal{M}_{n_0}^{[0,t)(i)}$ be the functional value (10) calculated along the ith trajectory. From the law of large numbers we have

$$\mathsf{E}\left(\mathcal{M}_{n_0}^{[0,t)}\right) = \lim_{N \to \infty} \frac{1}{N} \sum_{i=1}^{N} \mathcal{M}_{n_0}^{[0,t)(i)}. \tag{24}$$

5.2. Reconfigurations

Equation (10) represents a product of N_t random factors and, since N_t grows with t, the fluctuations of the functional $\mathcal{M}_{n_0}^{[0,t)}$ grow exponentially with t. This implies that the number of trajectories needed to have good statistical averages grows exponentially with t. A similar problem was successfully tackled some years ago in the framework of GFMC by the reconfiguration technique [8, 9]. This technique can be adapted also to the present probabilistic representation. In fact, for boson systems at imaginary times the stochastic functional $\mathcal{M}_{n_0}^{[0,t)}$ is always positive and can be thought of as a weight. Let us divide the time interval $[0, t)$ in R subintervals of the same length $\Delta t = t/R$. Let us label the times corresponding to the end points of these intervals as

$$t_r \equiv r\Delta t, \qquad r = 0, \dots, R \tag{25}$$

and let n_{t_r} be the configuration reached at the time $t_r + 0^+$ through the dynamics described in section 3 (we recall that the Poisson processes are left continuous defined). The following obvious identity follows from equation (10)

$$\mathcal{M}_{n_0}^{[0,t)} = \prod_{r=1}^{R} \mathcal{M}_{n_{t_{r-1}}}^{[t_{r-1},t_r)}, \tag{26}$$

which implies

$$\mathsf{E}\left(\mathcal{M}_{n_0}^{[0,t)}\right) = \mathsf{E}\left(\prod_{r=1}^{R} \mathcal{M}_{n_{t_{r-1}}}^{[t_{r-1},t_r)}\right). \tag{27}$$

The functional $\mathcal{M}_{n_{t_{r-1}}}^{[t_{r-1},t_r)}$ will be referred to as local weight.

Essentially, the idea of the reconfiguration technique is the following. Instead of extracting independent trajectories, one carries on an ensemble of M trajectories simultaneously in order to perform dynamically, at the times t_r, a suitable replica of those with large weights, eliminating at the same time the others. This replication/elimination of trajectories, also referred to as reconfiguration, has to be done in such a way that the number of trajectories M remains constant. At the end, one can substitute the average of $\prod_{r=1}^{R} \mathcal{M}_{n_{t_{r-1}}}^{[t_{r-1},t_r)}$ with the average of $\prod_{r=1}^{R} \langle \mathcal{M}_{\widetilde{n}_{t_{r-1}}}^{[t_{r-1},t_r)} \rangle$, where with $n_{t_r} \to \widetilde{n}_{t_r}$ we indicate the reconfiguration action at the time t_r, and with $\langle \mathcal{M}_{\widetilde{n}_{t_{r-1}}}^{[t_{r-1},t_r)} \rangle$ the uniform 'average' of the local weights over the M reconfigured trajectories (we use quotation marks since this quantity is itself a random variable). Hence, the remarkable advantage of using the reconfigurations is that, if the functional $\prod_{r=1}^{R} \mathcal{M}_{n_{t_{r-1}}}^{[t_{r-1},t_r)}$ has variance Δ^{R^*}, the variance of $\prod_{r=1}^{R} \langle \mathcal{M}_{\widetilde{n}_{t_{r-1}}}^{[t_{r-1},t_r)} \rangle$ will be roughly $(\Delta/\sqrt{M})^{R^*}$, where Δ is

the variance of the local weights and $R^* < R$ is the number of subintervals in which the local weights become approximately independent.

5.2.1. Reconfiguration algorithm. Here, we describe in detail the reconfiguration algorithm at imaginary times postponing the relative proof to the next section. We will indicate with $n_{t_r}^{(i)}, r = 0, \ldots, R$, and $\mathcal{M}_{n_{t_{r-1}}^{(i)}}^{[t_{r-1}, t_r)(i)}, r = 1, \ldots, R$, the configurations and the local weights of the *i*th trajectory and define the corresponding *M*-component vectors as $\underline{n}_{t_r}$ and $\mathcal{M}_{\underline{n}_{t_{r-1}}}^{[t_{r-1}, t_r)}$, respectively. We shall also use the operator symbols $\mathcal{D}$ and $\mathcal{R}$: $\mathcal{D}$ applied to the configurations $\underline{n}_{t_r}$ gives the configurations $\underline{n}_{t_{r+1}}$ according to the dynamics defined in section 3 along the time interval $[t_r, t_{r+1})$, whereas $\mathcal{R}$ gives the reconfigured configurations $\underline{\widetilde{n}}_{t_r} = \mathcal{R}\underline{n}_{t_r}$.

First step. Define $\underline{\widetilde{n}}_{t_0} = \underline{n}_{t_0}$ with $n_{t_0}^{(i)} = n_0$ for $i = 1, \ldots, M$. At the initial time $t_0 = 0$, all the *M* trajectories starting from the initial configuration n_0 follow the dynamics $\mathcal{D}$ and reach the configurations $\underline{n}_{t_1} = \mathcal{D}\underline{n}_{t_0}$. Correspondingly, evaluate the *M* local weights along the time interval $[0, t_1)$, $\mathcal{M}_{\underline{\widetilde{n}}_{t_0}}^{[0, t_1)}$, and compute their average

$$\langle \mathcal{M}_{\underline{\widetilde{n}}_{t_0}}^{[0, t_1)} \rangle \equiv \frac{1}{M} \sum_{l=1}^{M} \mathcal{M}_{\underline{\widetilde{n}}_{t_0}}^{[0, t_1)(l)}. \tag{28}$$

Second step. Perform the reconfiguration $\underline{n}_{t_1} \to \underline{\widetilde{n}}_{t_1} = \mathcal{R}\underline{n}_{t_1}$. The new configurations are obtained by drawing out them randomly from the old ones, $\underline{n}_{t_1}$, according to the probabilities

$$\mathcal{P}_{t_1}^{(i)} \equiv \frac{\mathcal{M}_{\underline{\widetilde{n}}_{t_0}}^{[0, t_1)(i)}}{\sum_{l=1}^{M} \mathcal{M}_{\underline{\widetilde{n}}_{t_0}}^{[0, t_1)(l)}}. \tag{29}$$

The new configurations $\underline{\widetilde{n}}_{t_1}$ are used as starting configurations of the *M* trajectories for the time interval $[t_1, t_2)$ and, through the dynamics $\mathcal{D}$, are mapped into $\mathcal{D}\underline{\widetilde{n}}_{t_1}$. Correspondingly, evaluate the *M* local weights $\mathcal{M}_{\underline{\widetilde{n}}_{t_1}}^{[t_1, t_2)}$ and compute their average

$$\langle \mathcal{M}_{\underline{\widetilde{n}}_{t_1}}^{[t_1, t_2)} \rangle \equiv \frac{1}{M} \sum_{l=1}^{M} \mathcal{M}_{\widetilde{n}_{t_1}^{(l)}}^{[t_1, t_2)(l)}. \tag{30}$$

Third step. Perform the reconfiguration $\mathcal{D}\underline{\widetilde{n}}_{t_1} \to \underline{\widetilde{n}}_{t_2} = \mathcal{R}\mathcal{D}\underline{\widetilde{n}}_{t_1}$ by drawing out the new configurations randomly from the old ones according to the probabilities

$$\mathcal{P}_{t_2}^{(i)} \equiv \frac{\mathcal{M}_{\widetilde{n}_{t_1}^{(i)}}^{[t_1, t_2)(i)}}{\sum_{l=1}^{M} \mathcal{M}_{\widetilde{n}_{t_1}^{(l)}}^{[t_1, t_2)(l)}}. \tag{31}$$

The new configurations $\underline{\widetilde{n}}_{t_2}$ are used as starting configurations in the time interval $[t_2, t_3)$. Evaluate the local weights $\mathcal{M}_{\underline{\widetilde{n}}_{t_2}}^{[t_2, t_3)}$ and compute their average

$$\langle \mathcal{M}_{\underline{\widetilde{n}}_{t_2}}^{[t_2, t_3)} \rangle \equiv \frac{1}{M} \sum_{l=1}^{M} \mathcal{M}_{\widetilde{n}_{t_2}^{(l)}}^{[t_2, t_3)(l)}. \tag{32}$$

By iterating this procedure for *R* steps, we arrive at the final configurations $\mathcal{D}\underline{\widetilde{n}}_{t_{R-1}} = \mathcal{D}(\mathcal{R}\mathcal{D})^{R-1}\underline{n}_{t_0}$, with *R* computed averages $\langle \mathcal{M}_{\underline{\widetilde{n}}_{t_{r-1}}}^{[t_{r-1}, t_r)} \rangle, r = 1, \ldots, R$. As we will prove later,

the following identity holds

$$E(\mathcal{M}_{n_0}^{[0,t)}) = \widetilde{E}\left(\prod_{r=1}^{R} \langle \mathcal{M}_{\widetilde{n}_{t_{r-1}}}^{[t_{r-1},t_r)} \rangle\right), \tag{33}$$

where $\widetilde{E}$ indicates the expectation in which the configurations $\widetilde{n}_{t_r}$ are obtained by the reconfiguration procedure described above. Explicitly, equation (33) implies that to evaluate the expectation $E(\mathcal{M}_{n_0}^{[0,t)})$, instead of equation (24), we can use

$$E(\mathcal{M}_{n_0}^{[0,t)}) = \lim_{M \to \infty} \prod_{r=1}^{R} \langle \mathcal{M}_{\widetilde{n}_{t_{r-1}}}^{[t_{r-1},t_r)} \rangle, \tag{34}$$

or, more generally, simulating N independent samples each one composed by M reconfigured trajectories,

$$E(\mathcal{M}_{n_0}^{[0,t)}) = \lim_{MN \to \infty} \frac{1}{N} \sum_{p=1}^{N} \prod_{r=1}^{R} \langle \mathcal{M}_{\widetilde{n}_{t_{r-1}}}^{[t_{r-1},t_r)} \rangle^{(p)}. \tag{35}$$

The label (p) in equation (35) means pth sample. Note that for $M = 1$ we recover equation (24).

All what we said about the functional $\mathcal{M}_{n_0}^{[0,t)}$ can be repeated for the functional $\mathcal{M}_{n_0}^{[0,t)}\delta_{n,n_t}$. In this case, equation (33) becomes

$$E(\mathcal{M}_{n_0}^{[0,t)}\delta_{n,n_t}) = \widetilde{E}\left(\prod_{r=1}^{R-1} \langle \mathcal{M}_{\widetilde{n}_{t_{r-1}}}^{[t_{r-1},t_r)} \rangle \frac{1}{M} \sum_{l=1}^{M} \mathcal{M}_{\widetilde{n}_{t_{R-1}}^{(l)}}^{[t_{R-1},t)(l)} \delta_{n,(\mathcal{D}\widetilde{n}_{t_{R-1}})^{(l)}}\right). \tag{36}$$

Equation (36) allows us to calculate the numerator of equation (15) as

$$E(\mathcal{M}_{n_0}^{[0,t)}\mathcal{H}(n_t)) = \widetilde{E}\left(\prod_{r=1}^{R-1} \langle \mathcal{M}_{\widetilde{n}_{t_{r-1}}}^{[t_{r-1},t_r)} \rangle \frac{1}{M} \sum_{l=1}^{M} \mathcal{M}_{\widetilde{n}_{t_{R-1}}^{(l)}}^{[t_{R-1},t)(l)} \mathcal{H}((\mathcal{D}\widetilde{n}_{t_{R-1}})^{(l)})\right). \tag{37}$$

5.2.2. Correlation functions. Let us now consider the reconfiguration procedure for the functionals introduced in equations (19) and (20) to obtain the correlation functions. In this case, we perform R steps in the first interval $[0, t)$ and R' steps in the second interval $[0, t')$. All the quantities relative to the second interval $[0, t')$ will be indicated with a prime. In the pure sampling, the initial configurations of the second interval $[0, t')$ are equal to the final ones of the first interval $[0, t)$: $\underline{n'_{t'_0}} = \underline{n_{t_R}}$. For diagonal operators, we have

$$E(\mathcal{M}_{n_t}'^{[0,t')} O(n_t) \mathcal{M}_{n_0}^{[0,t)}) = \widetilde{E}\left(\prod_{r=1}^{R} \langle \mathcal{M}_{\widetilde{n}_{t_{r-1}}}^{[t_{r-1},t_r)} \rangle \prod_{r'=1}^{R'-1} \langle \mathcal{M}_{\widetilde{n}'_{t'_{r'-1}}}'^{[t'_{r'-1},t'_{r'})} \rangle\right.$$
$$\left. \times \frac{1}{M} \sum_{l=1}^{M} \mathcal{M}_{\widetilde{n}'^{(l)}_{t'_{R'-1}}}'^{[t'_{R'-1},t')(l)} O((\mathcal{R}^{R'}\mathcal{D}\widetilde{n}_{t_{R-1}})^{(l)})\right), \tag{38}$$

where now the configurations $\mathcal{R}^{R'}\mathcal{D}\widetilde{n}_{t_{R-1}}$ are obtained by updating the intermediate configurations at time t_R, namely $\mathcal{D}\widetilde{n}_{t_{R-1}}$, R' times according to the successive R' steps. For off-diagonal operators, we have

$$E(\mathcal{M}_{n_t^{i\sigma \leftrightarrow j\sigma}}'^{[0,t')} O_{ij\sigma}(n_t) \mathcal{M}_{n_0}^{[0,t)}) = \widetilde{E}\left(\prod_{r=1}^{R} \langle \mathcal{M}_{\widetilde{n}_{t_{r-1}}}^{[t_{r-1},t_r)} \rangle \prod_{r'=1}^{R'-1} \langle \mathcal{M}_{\widetilde{n}'^{\mathrm{ex}}_{t'_{r'-1}}}'^{[t'_{r'-1},t'_{r'})} \rangle\right.$$
$$\left. \times \frac{1}{M} \sum_{l=1}^{M} \mathcal{M}_{\widetilde{n}'^{\mathrm{ex}(l)}_{t'_{R'-1}}}'^{[t'_{R'-1},t')(l)} O_{ij\sigma}((\mathcal{R}^{R'}\mathcal{D}\widetilde{n}_{t_{R-1}})^{(l)})\right), \tag{39}$$

where $\underline{\widetilde{\boldsymbol{n}}^{\mathrm{ex}}_{t_{r'-1}}}$, $r' = 1, \ldots, R'$, are the configurations obtained after r' steps starting from the intermediate configurations $\left(\mathcal{D}\widetilde{\boldsymbol{n}}_{t_{R-1}}\right)^{i\sigma \leftrightarrow j\sigma}$ in which the occupations of sites i and j with spin σ have been exchanged, i.e. $\underline{\widetilde{\boldsymbol{n}}^{\mathrm{ex}}_{t_{r'-1}}} = (\mathcal{RD})^{r'-1}\left(\mathcal{D}\widetilde{\boldsymbol{n}}_{t_{R-1}}\right)^{i\sigma \leftrightarrow j\sigma}$.

5.2.3. Real times. A reconfiguration procedure can be performed also at real times. In this case, the stochastic functional $\mathcal{M}^{[0,\mathrm{i}t)}_{\boldsymbol{n}_0}$ is complex and we separate the contributions from the R time intervals in their moduli and arguments, i.e.

$$\mathcal{M}^{[\mathrm{i}t_{r-1},\mathrm{i}t_r)}_{\boldsymbol{n}_{t_{r-1}}} = \left|\mathcal{M}^{[\mathrm{i}t_{r-1},\mathrm{i}t_r)}_{\boldsymbol{n}_{t_{r-1}}}\right| \mathrm{e}^{\mathrm{i}\Phi^{[t_{r-1},t_r)}_{\boldsymbol{n}_{t_{r-1}}}}, \tag{40}$$

where

$$\left|\mathcal{M}^{[\mathrm{i}t_{r-1},\mathrm{i}t_r)}_{\boldsymbol{n}_{t_{r-1}}}\right| = \mathrm{e}^{\int_{t_{r-1}}^{t_r} A(\boldsymbol{n}_s)\eta\,\mathrm{d}s}, \tag{41}$$

$$\Phi^{[t_{r-1},t_r)}_{\boldsymbol{n}_{t_{r-1}}} = \frac{\pi}{2}\left(N_{t_r} - N_{t_{r-1}}\right) - \int_{t_{r-1}}^{t_r} V(\boldsymbol{n}_s)\,\mathrm{d}s. \tag{42}$$

The moduli can be used as local weights for the reconfiguration operator $\mathcal{R}$. All the steps described in section 5.2.1 remain unchanged except for the last factor, which takes into account the R phase factors reconstructing the original stochastic functional. The final result is

$$\mathsf{E}\left(\mathcal{M}^{[0,\mathrm{i}t)}_{\boldsymbol{n}_0}\right) = \widetilde{\mathsf{E}}\left(\prod_{r=1}^{R-1}\langle\left|\mathcal{M}^{[\mathrm{i}t_{r-1},\mathrm{i}t_r)}_{\widetilde{\boldsymbol{n}}_{t_{r-1}}}\right|\rangle \frac{1}{M}\sum_{l=1}^{M}\left|\mathcal{M}^{[\mathrm{i}t_{R-1},\mathrm{i}t_R)(l)}_{\widetilde{\boldsymbol{n}}^{(l)}_{t_{R-1}}}\right| \mathrm{e}^{\mathrm{i}\sum_{r=1}^{R}\Phi^{[t_{r-1},t_r)(l)}_{(\mathcal{R}^{R-r}\underline{\widetilde{\boldsymbol{n}}_{t_{r-1}}})^{(l)}}}\right). \tag{43}$$

5.3. Importance sampling

Although the reconfiguration method controls the growth of the fluctuations of $\mathcal{M}^{[0,t)}$ along the trajectories, since the dimension of the Fock space grows exponentially with the lattice size, an extraction of the jumping links by importance sampling also may be mandatory to reduce the statistical errors of the local weights [6]. If some *a priori* approximation $|g\rangle$ of the ground state is known, which has the property $\langle\boldsymbol{n}|g\rangle \in \mathbb{R}\setminus 0$ for any Fock state $|\boldsymbol{n}\rangle$, then instead of sampling directly the operator $\exp(-Ht)$, it can be notably advantageous to sample the isospectral operator $\exp(-H_g t)$, where $\langle\boldsymbol{n}'|H_g|\boldsymbol{n}\rangle \equiv \langle\boldsymbol{n}'|g\rangle\langle\boldsymbol{n}'|H|\boldsymbol{n}\rangle\langle\boldsymbol{n}|g\rangle^{-1}$.

As explained in [4, 13], if $|g\rangle$ is a guiding function in the sense specified above, the generalization of the present algorithm to the case with importance sampling consists in replacing the number of active links, $A(\boldsymbol{n}) \equiv \sum_{(i,j)\in\Gamma}\sum_{\sigma=\uparrow\downarrow}|\lambda_{ij\sigma}(\boldsymbol{n})|$, in all the previous formulae with the quantity

$$A_g(\boldsymbol{n}) \equiv \sum_{(i,j)\in\Gamma}\sum_{\sigma=\uparrow\downarrow}\left|\lambda_{ij\sigma}(\boldsymbol{n})\frac{\langle\boldsymbol{n}\oplus\mathbf{1}_{i\sigma}\oplus\mathbf{1}_{j\sigma}|g\rangle}{\langle\boldsymbol{n}|g\rangle}\right|. \tag{44}$$

Correspondingly, the probability density for the jump times becomes

$$p_{A_g}(s) = A_g\eta\exp(-A_g\eta s), \tag{45}$$

and the extraction of the jumping link (i, j, σ) among the active ones must be performed according to the probabilities $|\langle\boldsymbol{n}\oplus\mathbf{1}_{i\sigma}\oplus\mathbf{1}_{j\sigma}|g\rangle\langle\boldsymbol{n}|g\rangle^{-1}|/A_g(\boldsymbol{n})$. Finally, the stochastic functional (10) is modified as

$$\mathcal{M}^{[0,t)}_{g,\boldsymbol{n}_0} = \mathrm{e}^{\int_0^t [A_g(\boldsymbol{n}_s)\eta - V(\boldsymbol{n}_s)]\,\mathrm{d}s}. \tag{46}$$

The advantage of using importance sampling becomes clear considering the local energy associated with H_g

$$\mathcal{H}_g(\boldsymbol{n}_t) \equiv \sum_{\boldsymbol{n}'} \langle \boldsymbol{n}'|g\rangle \langle \boldsymbol{n}'|H|\boldsymbol{n}_t\rangle \langle \boldsymbol{n}_t|g\rangle^{-1} = -[A_g(\boldsymbol{n}_t)\eta - V(\boldsymbol{n}_t)]. \tag{47}$$

In fact, in the limit $|g\rangle \to |E_0\rangle$ one has $\mathcal{H}_g(\boldsymbol{n}_t) \to E_0$ and accordingly $\mathcal{M}_{g,\boldsymbol{n}_0}^{[0,t)} \to \exp(-E_0 t)$ so that the fluctuations vanish.

For any choice of the guiding function $|g\rangle$, the modified stochastic functional (46) provides unbiased representations of the ground-state energy E_0 as well as of the expectation of a generic operator O in the ground state $|E_0\rangle$ of H. In fact, equation (15) now reads

$$\lim_{t\to\infty} \frac{\mathsf{E}\big(\mathcal{H}_g(\boldsymbol{n}_t)\mathcal{M}_{g,\boldsymbol{n}_0}^{[0,t)}\big)}{\mathsf{E}\big(\mathcal{M}_{g,\boldsymbol{n}_0}^{[0,t)}\big)} = E_{0g}, \tag{48}$$

where E_{0g} is the ground-state energy of H_g, which, however, is an operator isospectral to H. On the other hand, equation (18) written in terms of a g-modified operator O_g becomes

$$\lim_{t,t'\to\infty} \frac{\sum_{\boldsymbol{n}} \mathsf{E}\big(\mathcal{M}_{g,\boldsymbol{n}}^{\prime[0,t')}\langle \boldsymbol{n}|O_g|\boldsymbol{n}_t\rangle \mathcal{M}_{g,\boldsymbol{n}_0}^{[0,t)}\big)}{\mathsf{E}\big(\mathcal{M}_{g,\boldsymbol{n}_0}^{[0,t+t')}\big)} = \langle E_{0g}|O_g|E_{0g}\rangle. \tag{49}$$

By using $\langle \boldsymbol{n}|E_{0g}\rangle = \langle \boldsymbol{n}|g\rangle\langle \boldsymbol{n}|E_0\rangle$ and $\langle E_{0g}|\boldsymbol{n}\rangle = \langle \boldsymbol{n}|g\rangle^{-1}\langle E_0|\boldsymbol{n}\rangle$, it is simple to see that $\langle E_{0g}|O_g|E_{0g}\rangle = \langle E_0|O|E_0\rangle$ if we choose O_g as the operator defined by $\langle \boldsymbol{n}'|O_g|\boldsymbol{n}\rangle \equiv \langle \boldsymbol{n}'|g\rangle\langle \boldsymbol{n}'|O|\boldsymbol{n}\rangle\langle \boldsymbol{n}|g\rangle^{-1}$. Note that, in the case of diagonal operators, $O_g = O$.

Importance sampling may be useful also for a different purpose, namely the determination of the transition amplitudes $\langle g|e^{-iHt}|\boldsymbol{n}_0\rangle$ between two chosen states $|\boldsymbol{n}_0\rangle$ and $|g\rangle$. This is particularly interesting at real times and we illustrate the idea in this case. If $|g\rangle$ is a generic state with the property $\langle \boldsymbol{n}|g\rangle \in \mathbb{R} \setminus 0$ so that the isospectral Hamiltonian H_g is well defined, we have

$$\sum_{\boldsymbol{n}} \langle \boldsymbol{n}|e^{-iH_g t}|\boldsymbol{n}_0\rangle = \langle g|\boldsymbol{n}_0\rangle\langle g|e^{-iHt}|\boldsymbol{n}_0\rangle. \tag{50}$$

Since the expectation of the stochastic functional $\mathcal{M}_{\boldsymbol{n}_0}^{[0,it)}$ with the modified rules (44) and (45) provides an exact representation of the lhs of equation (50), we obtain the transition amplitudes $\langle g|e^{-iHt}|\boldsymbol{n}_0\rangle$ up to the constant $\langle g|\boldsymbol{n}_0\rangle$.

6. Proof of the reconfiguration algorithm

In this section, we prove equations (33)–(39). Let us consider an ensemble of M simultaneous trajectories obtained by the dynamics described in section 3 starting from the initial configuration $\boldsymbol{n}_0$. Let $P_R\big(\mathcal{M}_{\boldsymbol{n}_{t_0}}^{[t_0,t_1)}, \mathcal{M}_{\boldsymbol{n}_{t_1}}^{[t_1,t_2)}, \ldots, \mathcal{M}_{\boldsymbol{n}_{t_{R-1}}}^{[t_{R-1},t)}; \boldsymbol{n}_{t_0}, \boldsymbol{n}_{t_1}, \ldots, \boldsymbol{n}_{t_R}\big)$ be the probability density to have a realization in which the M trajectories have local weights $\mathcal{M}_{\boldsymbol{n}_{t_0}}^{[t_0,t_1)}, \mathcal{M}_{\boldsymbol{n}_{t_1}}^{[t_1,t_2)}, \ldots, \mathcal{M}_{\boldsymbol{n}_{t_{R-1}}}^{[t_{R-1},t)}$ and configurations $\boldsymbol{n}_{t_0}, \boldsymbol{n}_{t_1}, \ldots, \boldsymbol{n}_{t_R}$ at the times $t_0, t_1, \ldots, t_R$, respectively. For simplicity, here we shall often use $\mathcal{M}_{r-1}$ for $\mathcal{M}_{\boldsymbol{n}_{t_{r-1}}}^{[t_{r-1},t_r)}$ and $\boldsymbol{n}_r$ for $\boldsymbol{n}_{t_r}$. Since the M trajectories are independent, if we take $\boldsymbol{n}_0^{(l)} = \boldsymbol{n}_0$ for $l = 1, \ldots, M$, we have

$$\mathsf{E}\big(\mathcal{M}_{\boldsymbol{n}_0}^{[0,t)}\delta_{\boldsymbol{n},\boldsymbol{n}_t}\big) = \mathsf{E}\left(\prod_{r=1}^{R} \mathcal{M}_{r-1}\delta_{\boldsymbol{n},\boldsymbol{n}_R}\right) = \mathsf{E}\left(\frac{1}{M}\sum_{l=1}^{M}\prod_{r=1}^{R} \mathcal{M}_{r-1}^{(l)}\delta_{\boldsymbol{n},\boldsymbol{n}_R^{(l)}}\right). \tag{51}$$

Consider, then, the following identity,

$$\frac{1}{M}\sum_{l=1}^{M}\prod_{r=1}^{R}\mathcal{M}_{r-1}^{(l)}\delta_{n,n_R^{(l)}} = \left(\sum_{l=1}^{M}\mathcal{M}_0^{(l)}p_0^{(l)}\right)\left(\sum_{l=1}^{M}\mathcal{M}_1^{(l)}p_1^{(l)}\right)\cdots\left(\sum_{l=1}^{M}\mathcal{M}_{R-2}^{(l)}p_{R-2}^{(l)}\right)$$

$$\times\left(\sum_{l=1}^{M}\mathcal{M}_{R-1}^{(l)}\delta_{n,n_R^{(l)}}p_{R-1}^{(l)}\right),\tag{52}$$

where the quantities $\underline{p_0},\underline{p_1},\dots,\underline{p_{R-1}}$ are defined recursively by

$$\begin{cases} p_0^{(i)} = \dfrac{1}{M}\\[2mm] p_r^{(i)} = \dfrac{\mathcal{M}_{r-1}^{(i)}p_{r-1}^{(i)}}{\sum_{l=1}^{M}\mathcal{M}_{r-1}^{(l)}p_{r-1}^{(l)}}, \qquad r=1,\dots,R-1. \end{cases}\tag{53}$$

Equations (51) and (52) lead to

$$\mathsf{E}\left(\prod_{r=1}^{R}\mathcal{M}_{r-1}\delta_{n,n_R}\right) = \mathsf{E}\left(\prod_{r=1}^{R-1}\langle\mathcal{M}_{r-1}\rangle_w\langle\mathcal{M}_{R-1}\delta_{n,n_R}\rangle_w\right),\tag{54}$$

where the weighted 'averages', $\langle\mathcal{M}_r\rangle_w$ and $\langle\mathcal{M}_{R-1}\delta_{n,n_R}\rangle_w$, are defined as the weighted sums $\langle\mathcal{M}_r\rangle_w = \sum_{l=1}^{M}\mathcal{M}_r^{(l)}p_r^{(l)}$ and $\langle\mathcal{M}_{R-1}\delta_{n,n_R}\rangle_w = \sum_{l=1}^{M}\mathcal{M}_{R-1}^{(l)}\delta_{n,n_R^{(l)}}p_{R-1}^{(l)}$, respectively.

Up to now the quantities $\underline{p_r}$ have been thought of as stochastic variables. Actually, since the components $p_r^{(l)}$ are positive and normalized to 1, we can interpret them as probabilities to modify the original probability density P_R. We introduce a new probability density $\widetilde{P}_R$ that, besides taking into account the dynamics $\mathcal{D}^R$, includes the probabilities $\underline{p_r}$, for $r=0,\dots,R-1$. In this case, if we indicate with $\widetilde{\underline{n}}_0,\widetilde{\underline{n}}_1,\dots,\widetilde{\underline{n}}_{R-1},\mathcal{D}\widetilde{\underline{n}}_{R-1}$ the configurations extracted according to the probability density $\widetilde{P}_R$, equation (54) transforms into

$$\mathsf{E}\left(\prod_{r=1}^{R}\mathcal{M}_{r-1}\delta_{n,n_R}\right) = \widetilde{\mathsf{E}}\left(\prod_{r=1}^{R-1}\langle\mathcal{M}_{\widetilde{n}_{r-1}}^{[t_{r-1},t_r)}\rangle\frac{1}{M}\sum_{l=1}^{M}\mathcal{M}_{\widetilde{n}_{R-1}^{(l)}}^{[t_{R-1},t_R)(l)}\delta_{n,(\mathcal{D}\underline{\widetilde{n}}_{R-1})^{(l)}}\right),\tag{55}$$

where $\widetilde{\mathsf{E}}(\cdot)$ means expectation with respect to $\widetilde{P}_R$ and the weighted 'averages' $\langle\mathcal{M}_r\rangle_w$ have been substituted by uniform 'averages' over the new configurations, $\langle\mathcal{M}_{\widetilde{n}_{r-1}^{(l)}}^{[t_{r-1},t_r)}\rangle = \sum_{l=1}^{M}\mathcal{M}_{\widetilde{n}_{r-1}^{(l)}}^{[t_{r-1},t_r)(l)}/M$.

Equations (51) and (55) reproduce equation (36). To conclude the proof, we still have to show that the algorithm described in section 5.2.1 coincides with sampling the configurations $\widetilde{\underline{n}}_0,\widetilde{\underline{n}}_1,\dots,\widetilde{\underline{n}}_{R-1},\mathcal{D}\widetilde{\underline{n}}_{R-1}$ according to the probability density $\widetilde{P}_R$. For M trajectories with local weights $\mathcal{M}_{r-1}^{(i)}$, let us define the following probabilities:

$$\mathcal{P}_r^{(i)} = \frac{\mathcal{M}_{r-1}^{(i)}}{\sum_{l=1}^{M}\mathcal{M}_{r-1}^{(l)}}, \qquad r=1,\dots,R-1.\tag{56}$$

Due to the recursiveness of equation (53), for $r\geqslant 1$, we have

$$p_r^{(i)} = C_r\prod_{r'=1}^{r}\mathcal{P}_{r'}^{(i)},\tag{57}$$

where C_r is a normalization constant independent of the trajectory index (i). This allows us to realize the transformation $P_r\to\widetilde{P}_r$ recursively for $r=1,\dots,R$. At the first step $r=1$, since $\underline{p_0}$ is uniform we do not have to reconfigure and $\widetilde{\underline{n}}_0 = \underline{n}_0$. The density $\widetilde{P}_1$ will be

then sampled through the vectors $\widetilde{\underline{n}}_0$ and $\mathcal{D}\widetilde{\underline{n}}_0$. Suppose now we have sampled the density $\widetilde{P}_r$ through the vectors $\widetilde{\underline{n}}_0, \widetilde{\underline{n}}_1, \ldots, \widetilde{\underline{n}}_{r-1}, \mathcal{D}\widetilde{\underline{n}}_{r-1}$. To sample the density $\widetilde{P}_{r+1}$ we must change the arrival vector of configurations $\mathcal{D}\widetilde{\underline{n}}_{r-1}$ into a new vector $\widetilde{\underline{n}}_r$ according to the probabilities $\underline{\mathcal{P}}_r$, with components

$$\mathcal{P}_r^{(i)} = \frac{\mathcal{M}_{\widetilde{\underline{n}}_{t_{r-1}}}^{[t_{r-1},t_r)(i)}}{\sum_{l=1}^M \mathcal{M}_{\widetilde{\underline{n}}_{t_{r-1}}}^{[t_{r-1},t_r)(l)}}. \tag{58}$$

With a further step of the dynamics we get $\mathcal{D}\widetilde{\underline{n}}_r$. The distribution $\widetilde{P}_R$ is sampled by iterating this procedure R times. This is exactly the procedure explained in section 5.2.1 and the reconfiguration algorithm is proved.

Equation (33) follows easily by summing equation (36) over $\underline{n}$. Finally, equation (37) can be obtained multiplying $\mathcal{M}_{\underline{n}_0}^{[0,t)}\delta_{\underline{n},\underline{n}_t}$ by $\mathcal{H}(\underline{n})$ and then summing the product over $\underline{n}$.

Let us now consider the functional $\mathcal{M}_{\underline{n}_t}'^{[0,t')}\delta_{\underline{n},\underline{n}_t}\mathcal{M}_{\underline{n}_0}^{[0,t)}$. In analogy to the previous case, we easily arrive at

$$\mathsf{E}\left(\prod_{r=1}^R \mathcal{M}_{r-1}\delta_{\underline{n},\underline{n}_R} \prod_{r'=1}^{R'} \mathcal{M}'_{r'-1}\right) = \mathsf{E}\left(\prod_{r=1}^R \langle \mathcal{M}_{r-1}\rangle_w \prod_{r'=1}^{R'-1} \langle \mathcal{M}'_{r'-1}\rangle_w \langle \mathcal{M}'_{R'-1}\delta_{\underline{n},\underline{n}_R}\rangle_w\right), \tag{59}$$

where, recalling that $\underline{n}'_{t'_0} = \underline{n}_{t_R}$, the weighted 'averages' are given in terms of probabilities $\underline{p}_r$ defined recursively as in equation (53) with $r = 1, \ldots, R + R' - 1$. Let $P_{R+R'}$ and $\widetilde{P}_{R+R'}$ be the obvious extensions of the distributions P_R and $\widetilde{P}_R$ previously considered. As before, by using equations (56) and (57), for $r = 1, \ldots, R + R' - 1$, we can realize the transformation $P_{R+R'} \rightarrow \widetilde{P}_{R+R'}$ recursively: along the interval $[0, t)$ we sample $\widetilde{P}_1, \widetilde{P}_2, \ldots, \widetilde{P}_R$, whereas along $[0, t')$ we sample $\widetilde{P}_{R+1}, \widetilde{P}_{R+2}, \ldots, \widetilde{P}_{R+R'}$, obtaining the configurations $\widetilde{\underline{n}}_0, \widetilde{\underline{n}}_1, \ldots, \widetilde{\underline{n}}_R, \widetilde{\underline{n}}'_0, \widetilde{\underline{n}}'_1, \ldots, \widetilde{\underline{n}}'_{R'-1}, \mathcal{D}\widetilde{\underline{n}}'_{R'-1}$. Therefore, equation (59) transforms into

$$\mathsf{E}\left(\prod_{r=1}^R \mathcal{M}_{r-1}\delta_{\underline{n},\underline{n}_R} \prod_{r'=1}^{R'} \mathcal{M}'_{r'-1}\right) = \widetilde{\mathsf{E}}\left(\prod_{r=1}^R \langle \mathcal{M}_{\widetilde{\underline{n}}_{r-1}}^{[t_{r-1},t_r)}\rangle \prod_{r'=1}^{R'-1} \langle \mathcal{M}_{\widetilde{\underline{n}}'_{r'-1}}'^{[t_{r'-1},t_{r'})}\rangle\right.$$
$$\left. \times \frac{1}{M}\sum_{l=1}^M \mathcal{M}_{\widetilde{\underline{n}}'^{(l)}_{R'-1}}'^{[t_{R'-1},t_{R'})(l)}\delta_{\underline{n},(\mathcal{R}^{R'}\mathcal{D}\widetilde{\underline{n}}_{R-1})^{(l)}}\right), \tag{60}$$

which yields equation (38) after multiplying $\mathcal{M}_{\underline{n}_0}^{[0,t)}\delta_{\underline{n},\underline{n}_t}$ by $O(\underline{n})$ and then summing over $\underline{n}$. Note that on the rhs of equation (60) there appears $\mathcal{R}^{R'}\mathcal{D}\widetilde{\underline{n}}_{R-1}$ and not $\mathcal{D}\widetilde{\underline{n}}_{R-1}$. Indeed, according to equation (52), in the last weighted average $\langle \mathcal{M}'_{R'-1}\delta_{\underline{n},\underline{n}_R}\rangle_w = \sum_{l=1}^M \mathcal{M}'^{(l)}_{R'-1}\delta_{\underline{n}^{(l)}_R,\underline{n}}p^{(l)}_{R+R'-1}$ there appear the probabilities $\underline{p}_{R+R'-1}$ associated with the last time interval.

In general, in the reconfiguration procedure a weighted 'average'

$$\langle \mathcal{M}_{\underline{n}_{R-1}}^{[t_{R-1},t_R)}f(\underline{n}_0, \underline{n}_1, \ldots, \underline{n}_{R-1}, \underline{n}_R)\rangle_w \tag{61}$$

will be substituted by the uniform 'average'

$$\frac{1}{M}\sum_{l=1}^M \mathcal{M}_{\widetilde{\underline{n}}^{(l)}_{R-1}}^{[t_{R-1},t_R)(l)}f((\mathcal{R}^{R-1}\widetilde{\underline{n}}_0)^{(l)}, (\mathcal{R}^{R-2}\widetilde{\underline{n}}_1)^{(l)}, \ldots, (\mathcal{R}\widetilde{\underline{n}}_{R-1})^{(l)}, (\mathcal{D}\widetilde{\underline{n}}_{R-1})^{(l)}). \tag{62}$$

Equation (39) can be obtained in the same way as equation (38). Finally, in the case of real times, equation (43) is immediately obtained by using for the local weights the quantities

$\left| \mathcal{M}_{n_{t_{r-1}}}^{[it_{r-1}, it_r)} \right|$ and for the function $f(\cdot)$ of equation (62) the product of the phase factors

$$f = \prod_{r=1}^{R-1} e^{i\Phi_{n_{t_{r-1}}}^{[t_{r-1}, t_r)}}. \tag{63}$$

7. Numerical results

In this section, we present some numerical applications of the algorithm described above. In principle, the reconfiguration scheme can be applied for any positive integer R. However, we have observed optimal reconfiguration for $R \simeq \langle A \rangle \rho t$, where $\langle A \rangle$ is the average number of active links. This is what one expects as, in this case, the reconfiguration is repeated in the average at each jump, i.e. as frequently as the stochastic dynamics dictates (see also [14]). In the simulations reported below, therefore, we always work with this approximately optimal number of reconfigurations.

The count of the active links and of the potential of a given configuration, quantities to be determined at each jump, is a core point of the algorithm. Starting from a first count based on a systematic inspection of the initial lattice configuration, we have implemented a local updating of these quantities. In fact, when a jump occurs, the new Hubbard potential and the new number of active links are determined by the change of the lone occupations and of the lone links involved in the jump. The computational cost of a local update, which takes into account only these relevant sites and links, is independent of the lattice size. Also the reconfiguration procedure has been optimized by defining a non-negative integer, the replication multiplicity $\mu_r^{(i)}$, where (i) is the trajectory index and $\sum_{i=1}^M \mu_r^{(i)} = M$. Configurations for which $\mu_r^{(i)} = 0$ are substituted by those with $\mu_r^{(i)} > 1$, whereas no operation is performed for the trajectories with $\mu_r^{(i)} = 1$, which are the largest fraction of the whole set of M trajectories. The efficiency of the resulting code can be figured out by the following example. With an ordinary personal computer and without using importance sampling, we are able to simulate lattices with 40×40 sites with 800 hard-core bosons obtaining the ground-state energy up to a relative error of the order of 1% with 290 min of cpu time. A detailed comparison of the efficiency of our EPRMC code with those implementing other Monte Carlo methods is beyond the purposes of present work. In the appendix, we discuss the relative efficiency between EPRMC and GFMC or GFMCP.

In figures 1–5 we compare several quantities evaluated by the EPRMC algorithm with the corresponding exact results obtained by numerical diagonalization of the associated Hamiltonian. The system considered is a hard-core boson Hubbard model of small size, namely a 2×3 lattice at half-filling. The general purpose of these figures is to show the unbiased statistical convergence of the Monte Carlo data towards the exact values. No importance sampling is used in these first examples.

In figure 1 we show the expectation $\mathsf{E}\big(\mathcal{M}_{n_0}^{[0,t)} \big)$ as a function of the imaginary time t. The agreement with the corresponding quantum matrix element $\sum_n \langle n | e^{-Ht} | n_0 \rangle$ is excellent. The reconfiguration procedure is able to control completely the fluctuations growing with t so that the error bars, negligible on the scale used, do not increase by increasing the time. Similar results are obtained for different initial configurations n_0.

In figure 2 we show the expectation $\mathsf{E}\big(\mathcal{M}_{n_0}^{[0,it)} \big)$ as a function of the real time t. Also in this case there is an exact statistical convergence towards the quantum matrix element $\sum_n \langle n | e^{-iHt} | n_0 \rangle$. However, in this case the reconfiguration procedure is able to control only a part of the fluctuations, namely those related to the modulus of the functional $\mathcal{M}_{n_0}^{[0,it)}$. The fluctuations associated with the corresponding phase factor make the convergence harder and harder for large times.
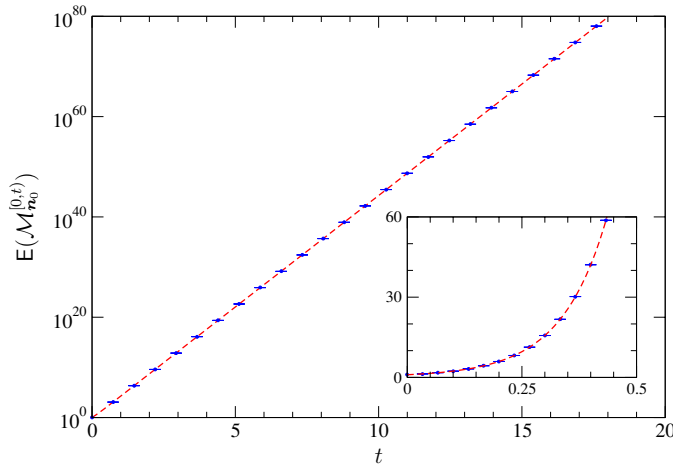
Figure 1. Expectation of the functional $\mathcal{M}_{n_0}^{[0,t)}$ versus the imaginary time t for a hard-core boson Hubbard system in a 2×3 lattice at half-filling with $\eta = 1, \gamma = 4$ and periodic boundary conditions. The initial configuration is $n_0 = (1, 1, 1, 0, 0, 0, 1, 1, 0, 1, 0, 0)$. The Monte Carlo simulation (dots with error bars) was done with $M = 2^{14}$ trajectories, $N = 2^7$ samples and $R = 300$ reconfigurations. Error bars correspond to one standard deviation evaluated from the N samples. The dashed line is the exact result from numerical diagonalization of the corresponding Hamiltonian. In the inset we show the small time behaviour.
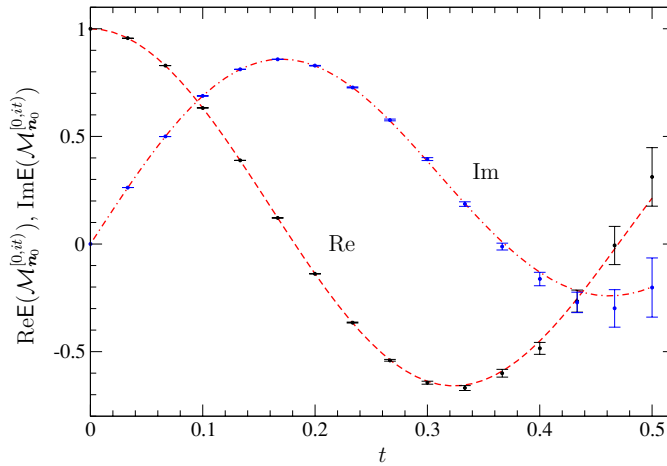

Figure 2. Expectation of the real and imaginary parts of the functional $\mathcal{M}_{n_0}^{[0,it)}$ versus the real time t for the same system of figure 1. The Monte Carlo simulation (dots with error bars) was done with $M = 2^{20}$ trajectories, $N = 2^7$ samples and $R = 15$ reconfigurations. Error bars correspond to one standard deviation evaluated from the N samples. The dashed (real part) and dot-dashed (imaginary part) lines are the exact results from numerical diagonalization.

In figure 3 we show the behaviour of the local energy $\mathsf{E}\big(\mathcal{M}_{n_0}^{[0,t)}\mathcal{H}(n_t)\big)\big/\mathsf{E}\big(\mathcal{M}_{n_0}^{[0,t)}\big)$ as a function of the imaginary time t. According to equation (15), the local energy converges to the ground-state energy of the system, E_0, for large times. In fact, after an initial transient inversely proportional to the gap $E_1 - E_0$, the ratio $\mathsf{E}\big(\mathcal{M}_{n_0}^{[0,t)}\mathcal{H}(n_t)\big)\big/\mathsf{E}\big(\mathcal{M}_{n_0}^{[0,t)}\big)$, estimated with a finite number of trajectories M, fluctuates around an average value that is close but
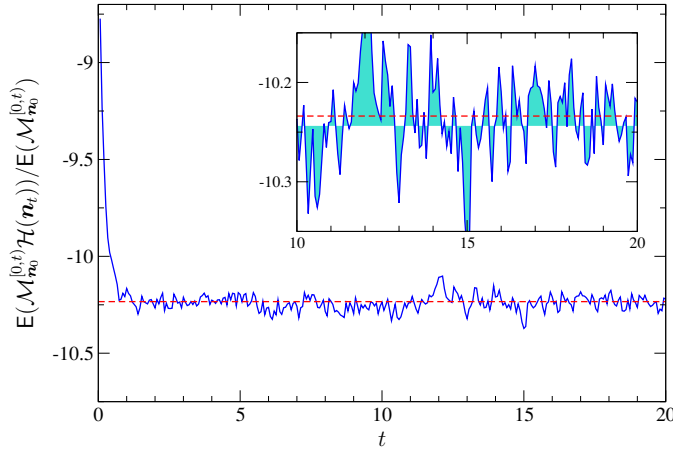
Figure 3. Local energy $\mathsf{E}(\mathcal{M}_{n_0}^{[0,t)}\mathcal{H}(\boldsymbol{n}_t))/\mathsf{E}(\mathcal{M}_{n_0}^{[0,t)})$ versus the imaginary time t for the same system of figure 1. The Monte Carlo simulation (solid line) was done with $M = 2^{14}$, $N = 1$ and $R = 300$. The straight dashed line is the exact energy $E_0 = -10.233\,803$ obtained by diagonalization. In the inset we evidence the difference between E_0 and the time average of $\mathsf{E}(\mathcal{M}_{n_0}^{[0,t)}\mathcal{H}(\boldsymbol{n}_t))/\mathsf{E}(\mathcal{M}_{n_0}^{[0,t)})$ computed over the interval $10 \leqslant t \leqslant 20$ (opaque region baseline).
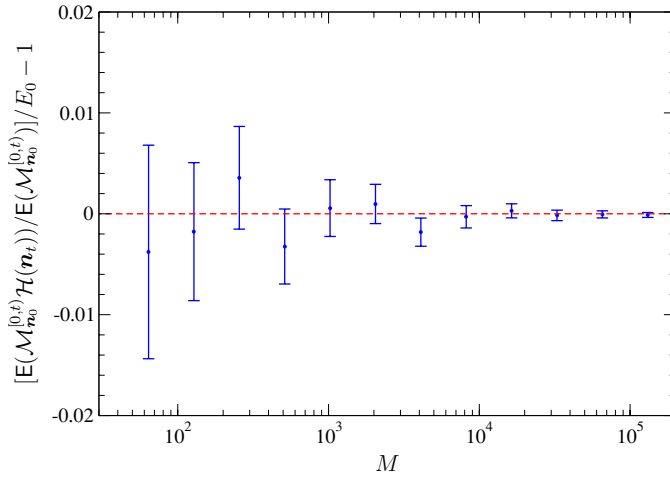
Figure 4. Relative error between the local energy $\mathsf{E}(\mathcal{M}_{n_0}^{[0,t)}\mathcal{H}(\boldsymbol{n}_t))/\mathsf{E}(\mathcal{M}_{n_0}^{[0,t)})$ and the exact energy E_0 versus the number M of reconfigured trajectories for the same system of figure 1 with $N = 2^7$, $t = 5$ and $R = 75$. Error bars correspond to two standard deviations evaluated from the N samples.

different from E_0 (see the inset of figure 3). However, if we increase M, as shown in figure 4, the statistical accuracy increases and we obtain an unbiased convergence towards E_0.

As an example of correlation functions, we have studied the spin–spin structure factor

$$S(q_x, q_y) = \frac{1}{|\Lambda|} \sum_{i,j \in \Lambda} \mathrm{e}^{\mathrm{i}q_x(x_i - x_j) + \mathrm{i}q_y(y_i - y_j)} \langle E_0 | S_i S_j | E_0 \rangle, \tag{64}$$

where $S_i = c_{i\uparrow}^\dagger c_{i\uparrow} - c_{i\downarrow}^\dagger c_{i\downarrow}$ and x_i and y_i are the coordinates of the ith lattice point. Note that the operators $S_i S_j$ are diagonal in the Fock space and can be evaluated by using equation (38).
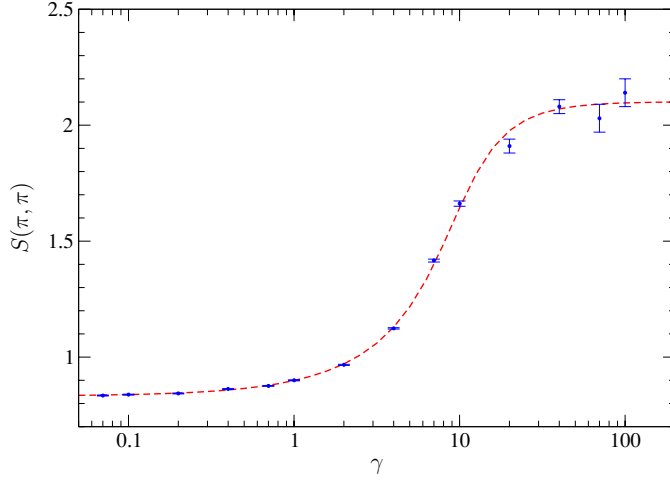
Figure 5. Spin–spin structure factor $S(q_x, q_y)$ at $q_x = q_y = \pi$ versus the interaction strength γ for the same system of figure 1. The dashed line is the exact result from numerical diagonalization of the Hamiltonian whereas the dots with error bars are from a Monte Carlo simulation with $M = 2^{14}$ ($M = 2^{18}$ for $\gamma > 10$), $N = 2^7$, $t = t' = 3$ and $R = 45$. Error bars correspond to one standard deviation evaluated from the N samples.

In figure 5 we show $S(\pi, \pi)$ evaluated for different values of the interaction strength γ. In agreement with the exact results from numerical diagonalization, $S(\pi, \pi)$ has a sharp transition between the $\gamma \to 0$ and $\gamma \to \infty$ asymptotic values. This transition is expected to take place when the average kinetic and potential energies are of the same order, i.e., for $\eta \langle A \rangle \sim \gamma \langle N_{\uparrow\downarrow} \rangle$, where $\langle N_{\uparrow\downarrow} \rangle$ is the average number of doubly occupied sites. For the system considered in figure 5, we have $\langle A \rangle \simeq 15$ and $\langle N_{\uparrow\downarrow} \rangle \simeq 1.5$ so that the transition is expected at $\gamma / \eta \sim 10$. This is in agreement with the numerical results.

In figure 6 we report simulations performed for hard-core boson Hubbard systems of large size. In particular, we show the local energy per site $\left[\mathsf{E}\big(\mathcal{M}_{n_0}^{[0,t)}\mathcal{H}(\boldsymbol{n}_t)\big) \big/ \mathsf{E}\big(\mathcal{M}_{n_0}^{[0,t)}\big) \right] / |\Lambda|$ as a function of the imaginary time t for two lattices at half-filling having size 20×20 and 40×40. Note that the standard deviations of the fluctuations around the long-time averaged value of $\left[\mathsf{E}\big(\mathcal{M}_{n_0}^{[0,t)}\mathcal{H}(\boldsymbol{n}_t)\big) \big/ \mathsf{E}\big(\mathcal{M}_{n_0}^{[0,t)}\big) \right] / |\Lambda|$ provide an estimated relative error for $E_0/|\Lambda|$ of the order of 1%. This result is obtained with a moderate computational effort. In figure 6 an asymmetry of the fluctuations of the local energy around its mean value is also evident. This behaviour is due to the reconfiguration procedure that ensures the invariance of the first statistical moment of $\mathcal{M}^{[0,t)}$ (or of related quantities) only.

We have performed simulations also for the Heisenberg model (5). In this case, we used importance sampling with the following Jastrow-like guiding state [9],

$$\langle \boldsymbol{n}|g \rangle \equiv \exp \left[\frac{\alpha}{2} \sum_{i,j \in \Lambda} \upsilon(\boldsymbol{r}_i - \boldsymbol{r}_j) \left(n_i - \frac{1}{2} \right) \left(n_j - \frac{1}{2} \right) \right], \tag{65}$$

where $\boldsymbol{r}_i = (x_i, y_i)$, α is a real positive parameter, and the long-range potential υ is defined as

$$\upsilon(\boldsymbol{r}) = \frac{2}{|\Lambda|} \sum_{(q_x, q_y) \neq (0,0)} \mathrm{e}^{\mathrm{i}q_x x + \mathrm{i}q_y y} \left[1 - \sqrt{\frac{1 + (\cos q_x + \cos q_y)/2}{1 - (\cos q_x + \cos q_y)/2}} \right], \tag{66}$$
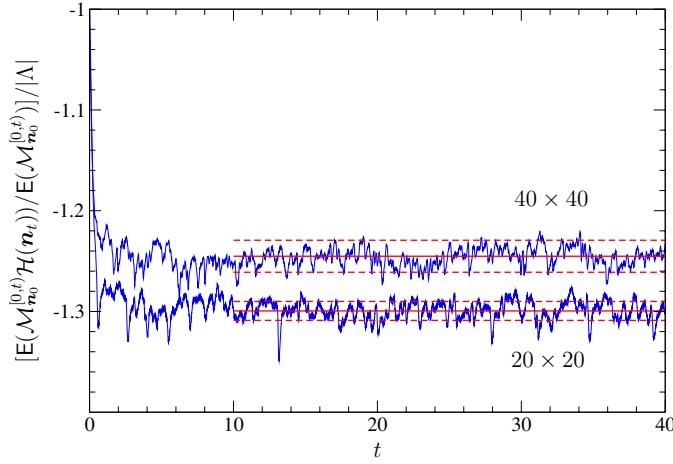
Figure 6. Local energy per site $[\mathsf{E}(\mathcal{M}_{n_0}^{[0,t)}\mathcal{H}(n_t))/\mathsf{E}(\mathcal{M}_{n_0}^{[0,t)})]/|\Lambda|$ versus the imaginary time t for two different-size hard-core boson Hubbard systems at half-filling with $\eta = 1$, $\gamma = 4$ and periodic boundary conditions. The Monte Carlo simulations (solid lines) were done with $M = 2^{12}$, $R = 2^{15}$, and $N = 1$. The straight solid lines are the time averages of the simulation results computed over the interval $10 \leqslant t \leqslant 40$ whereas the straight dashed lines indicate the relative standard deviations. The simulations took 79 (20×20 lattice) and 290 (40×40 lattice) min on a computer with a 2.40 GHz Intel Xeon CPU.

the sum over q_x and q_y being extended over the Brillouin zone $2\pi/L, 4\pi/L, \ldots, 2\pi$, with 0 excluded. From equation (65) we have

$$\frac{\langle n \oplus \mathbf{1}_k \oplus \mathbf{1}_l | g \rangle}{\langle n | g \rangle} = \exp\left[\alpha \sum_{i \in \Lambda, i \neq k, l} \left(n_i - \frac{1}{2}\right)[(n_k \oplus 1 - n_k)\upsilon(r_i - r_k)\right.$$

$$\left. + (n_l \oplus 1 - n_l)\upsilon(r_i - r_l)]\right]. \tag{67}$$

We assumed $\alpha = 1.2$ as suggested in [9].

In figure 7 we show the local energy per site $\left[\mathsf{E}\big(\mathcal{M}_{g,n_0}^{[0,t)}\mathcal{H}_g(n_t)\big)\big/\mathsf{E}\big(\mathcal{M}_{g,n_0}^{[0,t)}\big)\right]/|\Lambda|$ as a function of the imaginary time t for a 6×6 Heisenberg system having $\sum_{i=1}^{|\Lambda|} S_i^z = 0$. The amplitude of the error bars shown in figure 7 is considerably reduced with respect to the value that one would obtain without using importance sampling. We also stress that the dynamics shown in figure 7 is relative to the Hamiltonian H_g modified by the chosen guiding function $|g\rangle$.

In figure 8 we show the local staggered magnetization $\big\{3\big[\mathsf{E}\big(\mathcal{M}_{g,n_t}^{\prime[0,t')}S_{\pi\pi}^z(n_t)\mathcal{M}_{g,n_0}^{[0,t)}\big)\big/$ $\mathsf{E}\big(\mathcal{M}_{g,n_0}^{[0,t+t')}\big)\big]\big/|\Lambda|\big\}^{1/2}$ evaluated in Heisenberg systems of different size as a function of the imaginary time t' and for a large value of the other imaginary time t. Here $S_{\pi\pi}^z(n) = \langle n|S_{\pi\pi}^z|n\rangle$ is the quantum expectation in the Fock state n of the diagonal operator

$$S_{\pi\pi}^z = \frac{1}{|\Lambda|} \sum_{i,j \in \Lambda} \mathrm{e}^{\mathrm{i}\pi(x_i - x_j) + \mathrm{i}\pi(y_i - y_j)} S_i^z S_j^z. \tag{68}$$

As noted in the case of figure 7, also the dynamics of the local staggered magnetization shown in figure 8 is relative to the Hamiltonian H_g modified by the guiding function (67). The
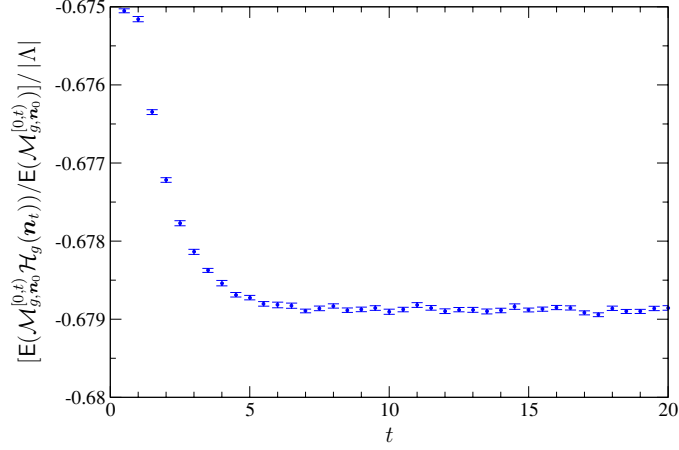
Figure 7. Local energy per site $[\mathsf{E}(\mathcal{M}_{g,n_0}^{[0,t]}\mathcal{H}_g(\boldsymbol{n}_t))/\mathsf{E}(\mathcal{M}_{g,n_0}^{[0,t]})]/|\Lambda|$ versus the imaginary time t for a 6×6 Heisenberg system with $\sum_{i=1}^{|\Lambda|} S_i^z = 0$ and $J = 1$. The Monte Carlo simulation (dots with error bars) was done by using importance sampling with the guiding function (67) and statistical parameters $M = 2^{16}$, $N = 2^6$ and $R = 20$.
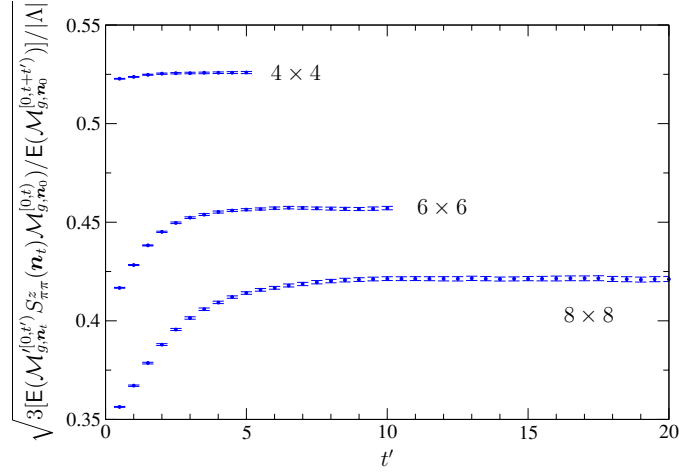

Figure 8. Local staggered magnetization $\{3[\mathsf{E}(\mathcal{M}_{g,n_t}'^{[0,t']} S_{\pi\pi}^z(\boldsymbol{n}_t)\mathcal{M}_{g,n_0}^{[0,t]})/\mathsf{E}(\mathcal{M}_{g,n_0}^{[0,t+t']})]/|\Lambda|\}^{1/2}$, defined in terms of the operator (68), versus the imaginary time t' for different-size Heisenberg systems with $\sum_{i=1}^{|\Lambda|} S_i^z = 0$ and $J = 1$. The Monte Carlo simulations (dots with error bars) were done by using importance sampling with the guiding function (67) with $\alpha = 1.2$ and parameters $t = 5$, $M = 2^{16}$, $N = 22$ and $R = 10$ in the 4×4 case, $t = 10$, $M = 2^{16}$, $N = 22$ and $R = 20$ in the 6×6 case, $t = 20$, $M = 2^{17}$, $N = 22$ and $R = 40$ in the 8×8 case.

asymptotic values of the local staggered magnetization reached for large t' are in agreement with those obtained with different Monte Carlo algorithms [9, 15]. The statistical errors shown in figure 8 can be reduced by a factor of about 10 by exploiting the covariance between the local estimators for $S_{\pi,\pi}^z$ and E_0, as explained in [15].

Finally, in figure 9 we provide an example of how the local expectation values shown in figure 8 depend on the parameter α of the guiding function (67). For different values of α the local expectations have different evolutions determined by $H_{g(\alpha)}$; however, as stated in
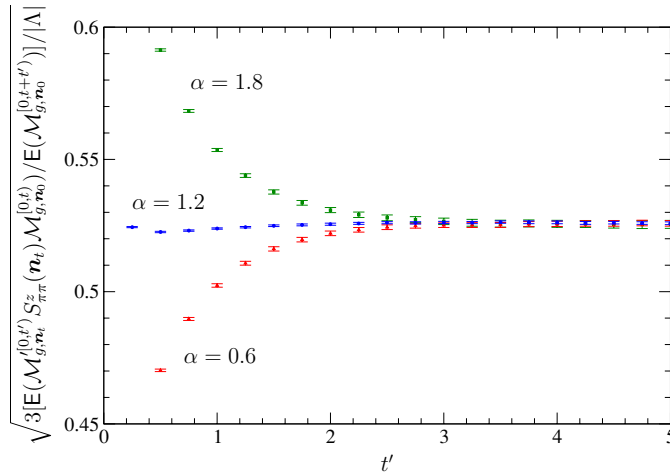
Figure 9. Local staggered magnetization versus the imaginary time t' for the 4×4 Heisenberg system of figure 8. The three curves were obtained with different values of the parameter α defining the importance sampling function (67). The other parameters were $t = 5$, $M = 2^{16}$, $N = 22$ and $R = 20$.

section 5.3 for a general guiding function, they all converge to the quantum expectation of $S^z_{\pi\pi}$ in the ground state of H. In agreement with [9], the value $\alpha = 1.2$ is close to the optimal choice, which provides smallest fluctuations and minimal evolution with respect to the asymptotic values.

In figures 1 and 2 we have shown that the imaginary- and real-time evolution of the expectation of the basic functional $\mathcal{M}^{[0,t)}_{n_0}$ coincides with that of the corresponding quantum matrix element $\sum_n \langle n | e^{-Ht} | n_0 \rangle$. Of course, a similar behaviour is general. Even if not shown explicitly, in all the considered examples the evolution of the relevant time-dependent probabilistic expectations coincides with that of the corresponding time-dependent quantum correlation functions.

8. Conclusions

We have exploited an exact probabilistic representation of the quantum dynamics in a lattice to derive a Monte Carlo algorithm, named EPRMC, for which standard fluctuation control techniques such as reconfigurations and importance sampling have been adapted and rigorously proved. This exact representation holds for both imaginary and real times, even if in the latter case only a partial fluctuation control is possible so that reliable statistical simulations are limited to short times.

Monte Carlo algorithms, such as GFMC or GFMCP, provide similar representations of the evolution operator, which are affected, however, by a systematic error ε controlled by the number of iterations performed. With respect to these approximated methods, EPRMC gives an efficiency gain proportional to the accuracy ε^{-1}.

Acknowledgment

Appendix

In this appendix, we calculate the relative efficiencies of GFMC and EPRMC methods. Both the methods have the aim to sample the operator e^{-Ht} for large t. We can write

$$U(t) = e^{-Ht} \sim e^{-E_0 t}, \qquad \text{for} \quad t \gg \bar{t}, \tag{A.1}$$

where $\bar{t}$ is the characteristic time to filter out the excited states $E_1, E_2, \ldots$ with respect to the ground state E_0,

$$\bar{t} = \frac{1}{E_1 - E_0}. \tag{A.2}$$

As explained in the introduction, GFMC samples the operator $(1 - Ht/N)^N$ whereas EPRMC samples directly the operator e^{-Ht}. Since $\lim_{N \to \infty}(1 + x/N)^N = e^x$, GFMC $\to$ EPRMC as the number of iterations N in the GFMC method grows. However, for a finite value of N, GFMC remains affected by a systematic error. We are interested in evaluating the critical value of N above which this error becomes smaller than a given value. Let us consider the relative difference

$$f_N(x) = \frac{e^x - \left(1 + \frac{x}{N}\right)^N}{e^x}. \tag{A.3}$$

By using

$$\log(1 + y) = \sum_{k=1}^{\infty} \frac{(-1)^{k+1}}{k} y^k, \tag{A.4}$$

equation (A.3) becomes

$$f_N(x) = \left(1 - e^{-\frac{x^2}{2N} + \frac{x^3}{3N^2} - \cdots}\right). \tag{A.5}$$

For concreteness, let us put $x = -E_0 t$ in equation (A.5). If we require that the relative error is $f_N(-E_0 t) = \varepsilon \ll 1$, then we must have $N \geqslant N_t(\varepsilon)$, where

$$N_t(\varepsilon) = \frac{E_0^2 t^2}{2\varepsilon}. \tag{A.6}$$

In conclusion, $N_t(\varepsilon)$ is the number of steps needed in GFMC to sample the operator e^{-Ht} for large t with a relative error equal to ε. On the other hand, the number of steps needed in EPRMC to sample e^{-Ht} for large t is given by the average number of jumps that, when an optimal reconfiguration scheme is chosen as discussed in section 7, coincides with the number of reconfigurations R_t

$$R_t = \langle A \rangle \eta t \simeq E_0^{(0)} t, \tag{A.7}$$

where $\langle A \rangle$ is the average number of active links and $E_0^{(0)}$ is the ground-state energy in the non-interacting case. Therefore, the relative efficiency of EPRMC with respect to GFMC is given by the ratio

$$\frac{N_t(\varepsilon)}{R_t} = \frac{E_0^2 t}{2 E_0^{(0)} \varepsilon}. \tag{A.8}$$

We see that the superiority of EPRMC grows by increasing the time t or increasing the accuracy ε^{-1} required in GFMC. In particular for $t = \bar{t}$ we have

$$\frac{N_{\bar{t}}(\varepsilon)}{R_{\bar{t}}} = \frac{E_0^2}{2 E_0^{(0)} (E_1 - E_0) \varepsilon}. \tag{A.9}$$

It is clear that if, instead of GFMC, we consider the GFMCP method, the efficiency ratio (A.8) changes. In fact, any step in GFMCP, on the average, amounts to $\langle n_s \rangle$ elementary GFMC steps, where roughly $\langle n_s \rangle = \langle A \rangle \eta t$ [4]. Thus, in GFMCP the number of steps needed to sample the operator e^{-Ht} for large t with a relative error ε is reduced to $N_t(\varepsilon) = E_0^2 t / \left(2 E_0^{(0)} \varepsilon\right)$ so that the relative efficiency of EPRMC with respect to GFMCP is given by the ratio

$$\frac{N_t(\varepsilon)}{R_t} = \left(\frac{E_0}{E_0^{(0)}}\right)^2 \frac{1}{2\varepsilon}. \tag{A.10}$$

This ratio no longer depends on t but remains proportional to the accuracy required in GFMCP.

References

[1]	von der Linden W 1992 *Phys. Rep.* **220** 53
[2]	De Angelis G F, Jona-Lasinio G and Sirugue M 1983 *J. Phys. A: Math. Gen.* **16** 2433
[3]	De Angelis G F, Jona-Lasinio G and Sidoravicius V 1998 *J. Phys. A: Math. Gen.* **31** 289
[4]	Beccaria M, Presilla C, De Angelis G F and Jona Lasinio G 1999 *Europhys. Lett.* **48** 243
[5]	Ostilli M and Presilla C 2004 *New J. Phys.* **6** 107
[6]	Ceperley D M and Kalos M H 1992 *Monte Carlo Methods in Statistical Physics* ed K Binder (Heidelberg: Springer)
[7]	Trivedi N and Ceperley D M 1990 *Phys. Rev.* B **41** 4552
[8]	Hetherington J H 1984 *Phys. Rev.* A **30** 2713
[9]	Calandra Buonaura M and Sorella S 1998 *Phys. Rev.* B **57** 11446
[10]	Beccaria M 2000 *Eur. Phys. J.* C **13** 357
[11]	Hubbard J 1963 *Proc. R. Soc.* A **276** 238
[12]	Matsubara T and Matsuda H 1956 *Prog. Theor. Phys.* **16** 569
[13]	Beccaria M, Presilla C, De Angelis G F and Jona Lasinio G 2001 *Int. J. Mod. Phys.* **15** 1740
[14]	Assaraf R, Caffarel M and Khelif A 2000 *Phys. Rev.* E **61** 4566
[15]	Sandvik A 1997 *Phys. Rev.* B **56** 11678